

Intertwined quantum phase transitions in odd-mass Nb isotopes

A. Leviatan^{1,*}, N. Gavrielov^{2,3,**}, and F. Iachello^{3,***}

¹Racah Institute of Physics, The Hebrew University, Jerusalem 91904, Israel

²Grand Accélérateur National d'Ions Lourds, CEA/DRF-CNRS/IN2P3, Bvd Henri Becquerel, BP 55027, F-14076 Caen, France

³Center for Theoretical Physics, Sloane Physics Laboratory, Yale University, New Haven, Connecticut 06520-8120, USA

Abstract. A detailed analysis of odd-mass Nb isotopes, in the framework of the interacting boson-fermion model with configuration mixing, discloses the effects of an abrupt crossing of states in normal and intruder configurations (Type II QPT), on top of which superimposed a gradual evolution from spherical- to deformed-core shapes within the intruder configuration (Type I QPT). The pronounced presence of both types of QPTs demonstrates, for the first time, the occurrence of intertwined QPTs in odd-mass nuclei.

1 Introduction

Structural changes induced by variation of parameters in the Hamiltonian, called quantum phase transitions (QPTs), are currently a topic of great interest in nuclear physics. In this field, most of the attention has been devoted to the evolution of structure with nucleon number, exhibiting two types of phase transitions. The first, denoted as Type I [1], is a shape-phase transition within a single configuration, as encountered in the neutron number 90 region [2]. The second, denoted as Type II [3], is a phase transition involving a crossing of different configurations, as encountered in nuclei near (sub-) shell closure [4]. In most cases, the strong mixing between the configurations obscures the individual QPTs. However, if the mixing is small, the Type II QPT can be accompanied by a distinguished Type I QPT within each configuration separately. Such a scenario, referred to as intertwined QPTs, was recently shown to occur in the even-even Zr ($Z=40$) isotopes [5–7]. In the present contribution, we show that a similar scenario occurs in the adjacent odd-even Nb ($Z=41$) isotopes [8, 9].

2 IBFM with configuration mixing

Odd- A nuclei are treated in the interacting boson-fermion model (IBFM) [10], as a system of monopole (s) and quadrupole (d) bosons, representing valence nucleon pairs, and a single (unpaired) nucleon. The corresponding Hamiltonian has the form

$$\hat{H} = \hat{H}_b + \hat{H}_f + \hat{V}_{bf}. \quad (1)$$

For a single configuration, the boson part involves an interacting boson model (IBM) [11] Hamiltonian, taken to be $\hat{H}_b(\epsilon_d, \kappa, \chi) = \epsilon_d \hat{n}_d + \kappa \hat{Q}_\chi \cdot \hat{Q}_\chi$, where $\hat{n}_d = \sum_m d_m^\dagger d_m$,

$\hat{Q}_\chi = d^\dagger s + s^\dagger \tilde{d} + \chi (d^\dagger \tilde{d})^{(2)}$ and $\tilde{d}_m = (-1)^m d_{-m}$. The control parameters $(\epsilon_d, \kappa, \chi)$ interpolate between the U(5) [spherical vibrator], SU(3) [axial rotor] and SO(6) [γ -unstable rotor] dynamical symmetry limits of the IBM. The fermion part involves the single-particle term, $\hat{H}_f = \sum_j \epsilon_j \hat{n}_j$. The boson-fermion part involves monopole, quadrupole and exchange terms, $\hat{V}_{bf} = \hat{V}_{bf}^{\text{MON}} + \hat{V}_{bf}^{\text{QUAD}} + \hat{V}_{bf}^{\text{EXC}}$. For a single- j fermion, $\hat{V}_{bf}^{\text{MON}} = A \hat{n}_d \hat{n}_j$, $\hat{V}_{bf}^{\text{QUAD}} = \Gamma \hat{Q}_\chi \cdot (a_j^\dagger \tilde{a}_j)^{(2)}$, $\hat{V}_{bf}^{\text{EXC}} = \Lambda \sqrt{2j+1} : [(d^\dagger \tilde{a}_j)^{(j)} \times (\tilde{d} a_j^\dagger)^{(j)}]^{(0)} :$ where $\tilde{a}_{j,m} = (-1)^{j+m} a_{j,-m}$ and $::$ denotes normal ordering. The IBM and IBFM Hamiltonians, $\hat{H}_b(\epsilon_d, \kappa, \chi)$ and \hat{H} of Eq. (1), have been used extensively in the study of Type I QPTs in even-even nuclei [2, 12–14] and odd-even nuclei [10, 15–20]), respectively.

For two configurations (A,B), the Hamiltonian of the interacting boson-fermion model with configuration mix-

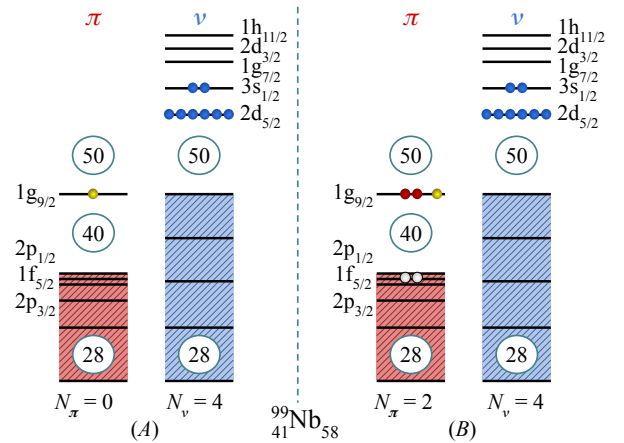


Figure 1. Schematic representation of the two coexisting shell-model configurations (A and B) for $^{99}\text{Nb}_{58}$. The corresponding numbers of proton bosons (N_π) and neutron bosons (N_v), are listed for each configuration and $N = N_\pi + N_v$.

*e-mail: ami@phys.huji.ac.il

**e-mail: noam.gavrielov@ganil.fr

***e-mail: francesco.iachello@yale.edu

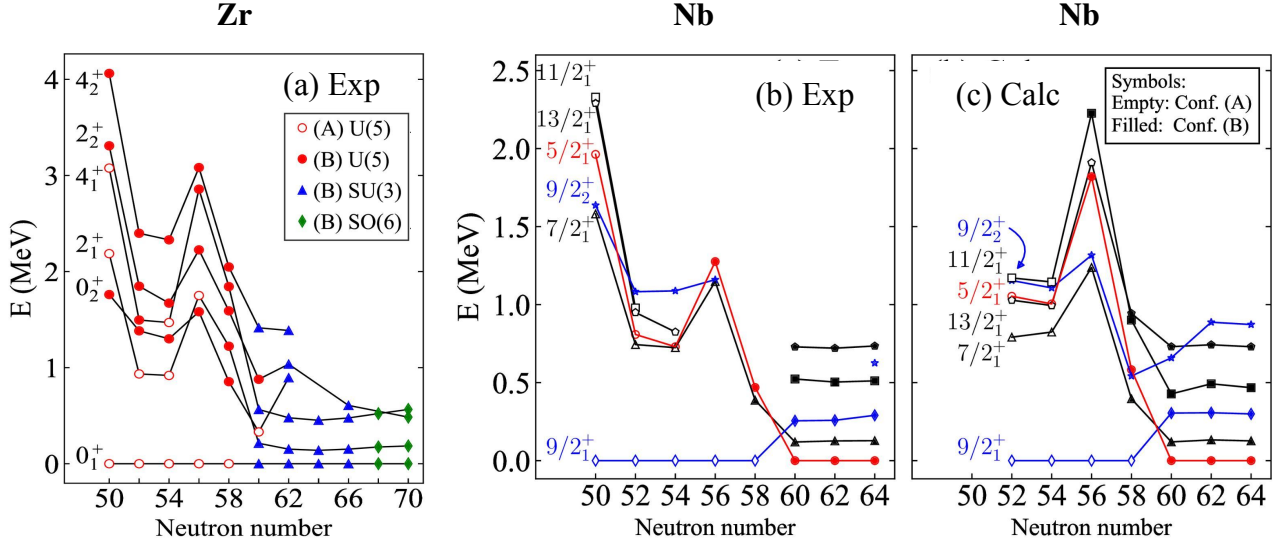


Figure 2. Comparison between experimental and calculated lowest-energy positive-parity levels in Zr [panel (a)] and Nb isotopes [panels (b) and (c)]. Empty (filled) symbols indicate a state dominated by the normal A configuration (intruder B configuration). In particular, the 0_1^+ state for Zr and the $9/2_1^+$ state for Nb, are assigned to the A (B) configuration for neutron number 52–58 (at and beyond 60). In panel (a), the shape of the symbol [\circ , \triangle , \diamond], indicates the closest dynamical symmetry [U(5), SU(3), SO(6)] to the level considered. Note that the calculated values start at 52, while the experimental values include the closed shell at 50.

ing (IBFM-CM) can be cast in matrix form [8],

$$\hat{H} = \begin{bmatrix} \hat{H}_b^A + \hat{H}_f + \hat{V}_{bf} & \hat{W}_b + \hat{W}_{bf} \\ \hat{W}_b + \hat{W}_{bf} & \hat{H}_b^B + \hat{H}_f + \hat{V}_{bf} \end{bmatrix}. \quad (2)$$

Here $\hat{H}_b^A = \hat{H}_b(\epsilon_d^{(A)}, \kappa^{(A)}, \chi)$ represents the normal A configuration (N boson space) and $\hat{H}_b^B = \hat{H}_b(\epsilon_d^{(B)}, \kappa^{(B)}, \chi) + \kappa^{(B)} \hat{L} \cdot \hat{L} + \Delta_p$, with an added rotational term, represents the intruder B configuration ($N+2$ boson space), corresponding to 2p-2h excitations across the (sub-) shell closure. For simplicity, \hat{H}_f and \hat{V}_{bf} are taken to be the same in both configurations. The boson- and boson-fermion mixing terms are $\hat{W}_b + \hat{W}_{bf} = [\omega + \sum_j \omega_j \hat{n}_j] [(d^\dagger d^\dagger)^{(0)} + (s^\dagger)^2 + \text{H.c.}]$, where H.c. stands for Hermitian conjugate. For $\hat{H}_f = \hat{V}_{bf} = \hat{W}_b = \hat{W}_{bf} = 0$, the IBFM-CM Hamiltonian of Eq. (2) reduces to that of the IBM-CM model [21, 22], widely used in the study of configuration-mixed QPTs and shape-coexistence in even-even nuclei [5–7, 21–27].

The eigenstates of \hat{H} (2), $|\Psi; J\rangle$, are linear combinations of wave functions Ψ_A and Ψ_B , involving bosonic basis states in the two spaces $|[N], \alpha, L\rangle$ and $|[N+2], \alpha, L\rangle$. Here α denote additional quantum numbers of the dynamical symmetry chain. The boson (L) and fermion (j) angular momenta are coupled to J , $|\Psi; J\rangle = \sum_{\alpha, L, j} C_{\alpha, L, j}^{(N, J)} |\Psi_A; [N], \alpha, (L \otimes j) J\rangle + \sum_{\alpha, L, j} C_{\alpha, L, j}^{(N+2, J)} |\Psi_B; [N+2], \alpha, (L \otimes j) J\rangle$. The probability of normal-intruder mixing is given by

$$a^2 = \sum_{\alpha, L, j} |C_{\alpha, L, j}^{(N, J)}|^2, \quad b^2 = \sum_{\alpha, L, j} |C_{\alpha, L, j}^{(N+2, J)}|^2 = 1 - a^2. \quad (3)$$

The $E2$ operator for a single- j fermion has the form $\hat{T}(E2) = e^{(A)} \hat{Q}_\chi^{(N)} + e^{(B)} \hat{Q}_\chi^{(N+2)} + e_f (a_j^\dagger \tilde{a}_j)^{(2)}$, where the superscript (N) denotes a projection onto the $[N]$ boson space and ($e^{(A)}, e^{(B)}, e_f$) are effective charges. The parameters of the IBFM-CM Hamiltonian and transition operators are determined from a fit in the manner described in [8, 9].

3 QPTs in the Niobium chain

The ${}_{41}^A\text{Nb}$ isotopes with mass number $A=93$ –105 are described by coupling a proton to their respective ${}_{40}\text{Zr}$ cores with neutron number 52–64 (boson numbers $N=1$ –7). In the latter, the normal A configuration corresponds to having no active protons above the $Z=40$ sub-shell gap, and the intruder B configuration corresponds to two-proton excitation from below to above this gap, creating 2p-2h states. In the present contribution, we focus on the positive-parity states in the Nb isotopes [8] (both parity states are addressed in [9]). Such a case, reduces to a single- j calculation, with the $\pi(1g_{9/2})$ orbit coupled to the boson core. The IBFM-CM model space employed, consists of a single-fermion plus $[N] \oplus [N+2]$ boson spaces with $N=1, 2, \dots, 7$ for ${}^{93-105}\text{Nb}$. The two configurations relevant for ${}^{99}\text{Nb}$ are shown schematically in Fig. 1.

Figures 2(b) and 2(c) show the experimental and calculated levels of selected states in the Nb isotopes along with assignments to configurations based on Eq. (3). Empty (filled) symbols indicate a dominantly normal (intruder) state with small (large) b^2 probability. In the region between neutron number 50 and 56, there appear to be two sets of levels with weakly deformed structure, associated with configurations A and B. All levels decrease in energy for 52–54, away from closed shell, and rise again at 56 due to the $\nu(2d_{5/2})$ subshell closure. From 58, there is a pronounced drop in energy for the states of the B configuration. At 60, the two configuration cross, indicating a Type II QPT, and the ground state changes from $9/2_1^+$ to $5/2_1^+$, becoming the bandhead of a $K=5/2^+$ rotational band composed of $5/2_1^+, 7/2_1^+, 9/2_1^+, 11/2_1^+, 13/2_1^+$ states. The intruder B configuration remains strongly deformed and the band structure persists beyond 60. As shown in Fig. 2(a), a similar trend is encountered in the even-even Zr isotopes with the same neutron numbers, where

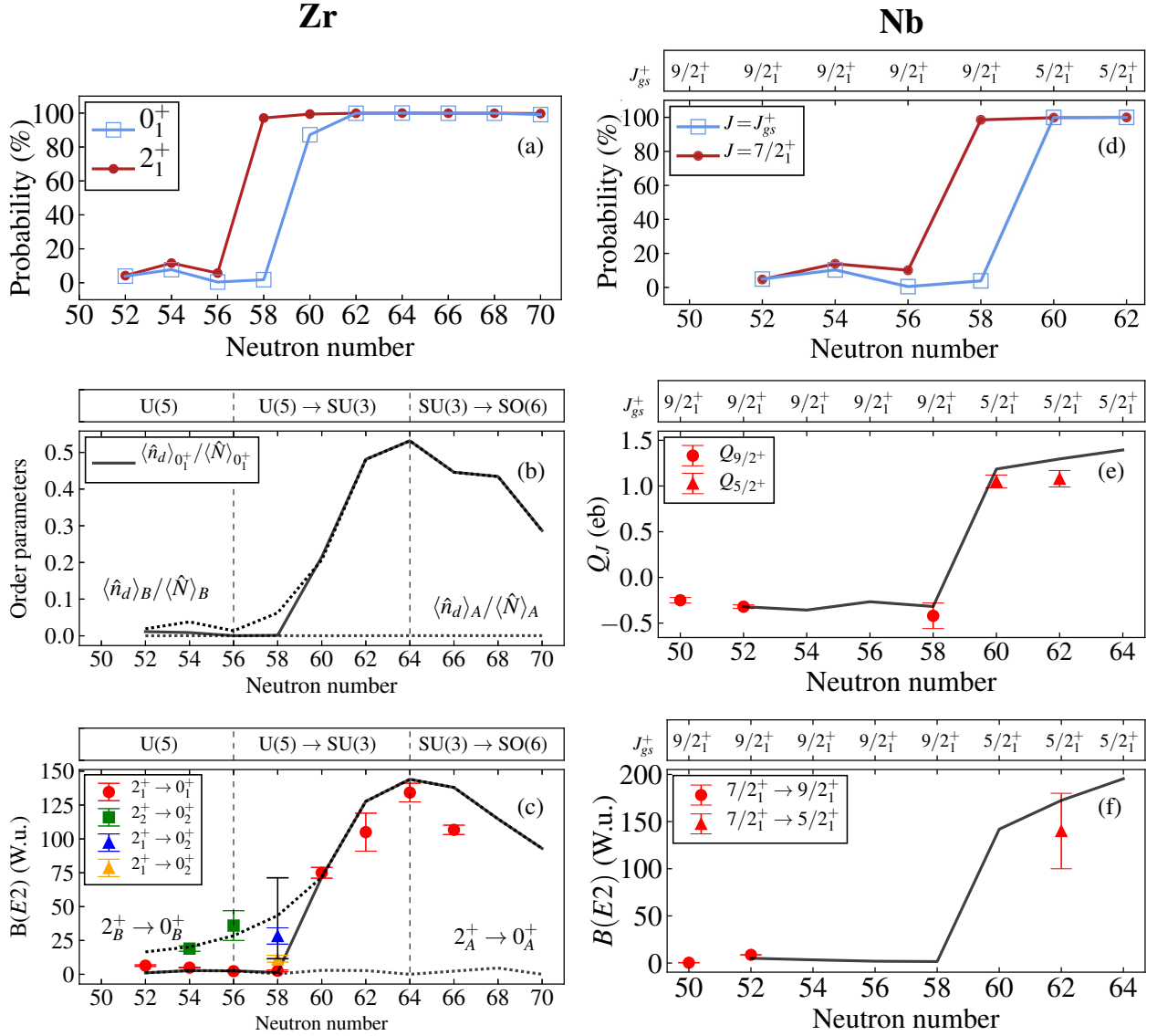


Figure 3. Evolution of spectral properties along the Zr and Nb chains. Symbols (solid lines) denote experimental data (calculated results). Left panels $^{92-110}\text{Zr}$ isotopes. (a) Percentage of the wave function within the intruder B-configuration for the ground (0_1^+) and excited (2_1^+) states. (b) Normalized order parameters (see text for details). (c) $B(E2)$ values for $2^+ \rightarrow 0^+$ transitions in Weisskopf units (W.u.). Dotted lines denote calculated $E2$ transitions within a configuration. For the data, see Fig. 17 of [7]. Right panels $^{93-105}\text{Nb}$ isotopes. (d) Percentage of the intruder (B) component [the b^2 probability in Eq. (3)], in the ground state (J_{gs}^+) and the first-excited positive-parity state ($7/2_1^+$). The values of J_{gs}^+ are indicated at the top. (e) Quadrupole moments of J_{gs}^+ in eb. (f) $B(E2; 7/2_1^+ \rightarrow J_{gs}^+)$ in W.u. For the data, see Fig. 12 of [8].

the spherical-to-deformed Type I QPT within the intruder configuration is associated with U(5)-SU(3) transition and subsequently SU(3)-SO(6) crossover [5–7].

A possible change in the angular momentum of the ground state (J_{gs}^+) is a characteristic signature of Type II QPTs in odd-mass, unlike even-even nuclei where the ground state remains 0^+ after the crossing. It is an important measure for the quality of the calculations, since a mean-field approach, without configuration mixing, fails to reproduce the switch from $9/2_1^+$ to $5/2_1^+$ in J_{gs}^+ for the Nb isotopes [28]. Fig. 3(d) shows the percentage of the wave function within the B configuration for J_{gs}^+ and $7/2_1^+$, as a function of neutron number across the Nb chain. The rapid change in structure of J_{gs}^+ from the normal A configuration in $^{93-99}\text{Nb}$ (small b^2 probability) to the intruder B config-

uration in $^{101-105}\text{Nb}$ (large b^2) is clearly evident, signaling a Type II QPT. The configuration change appears sooner in the $7/2_1^+$ state, which changes to the B configuration already in ^{99}Nb . Outside a narrow region near neutron number 60, where the crossing occurs, the two configurations are weakly mixed and the states retain a high level of purity. As shown in Fig. 3(a), a similar trend is encountered for the 0_1^+ and 2_1^+ states in the respective ^{40}Zr cores.

Further insight into the nature of the QPTs is gained by considering the behaviour of the order parameters and related observables. The quadrupole moment of J_{gs}^+ and $B(E2; 7/2_1^+ \rightarrow J_{gs}^+)$ in Nb isotopes are shown in Fig. 3(e) and Fig. 3(f), respectively. These observables are related to the deformation, the order parameter of the QPT. Although the data is incomplete, one can still observe small

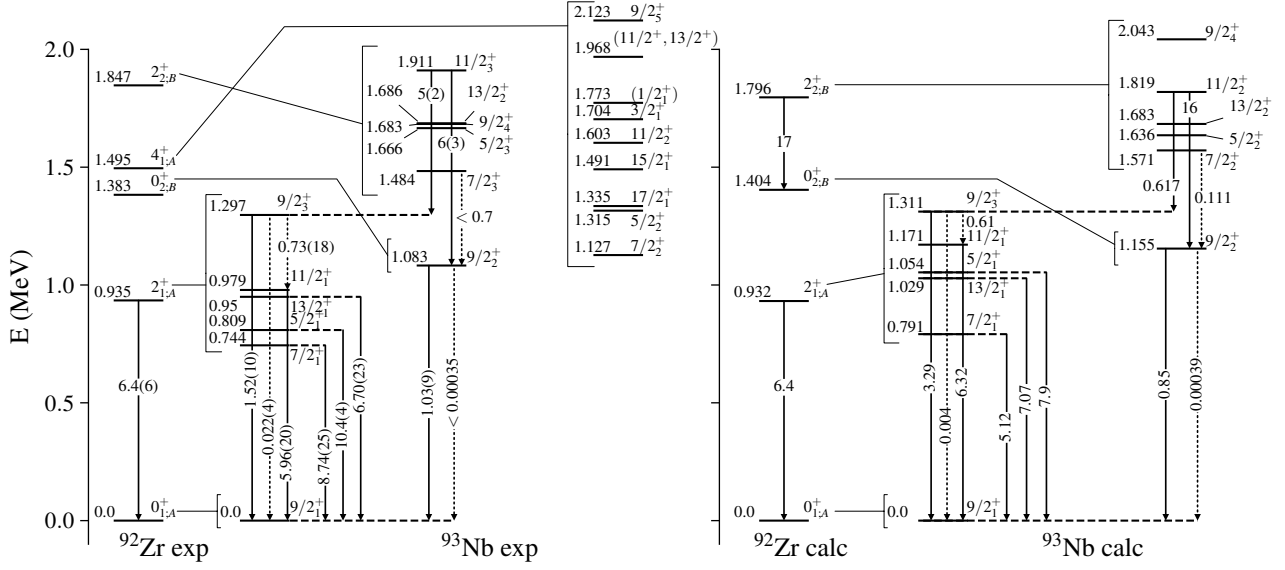


Figure 4. Experimental (left) and calculated (right) energy levels in MeV, and $E2$ (solid arrows) and $M1$ (dashed arrows) transition rates in W.u., for ^{93}Nb and ^{92}Zr . Lines connect L -levels in ^{92}Zr to sets of J -levels in ^{93}Nb , indicating the weak coupling ($L \approx \frac{9}{2}J$). For the data, see Fig. 3 of [8]. Note that the observed 4^+_{1A} state in ^{92}Zr is outside the $N=1$ model space.

(large) values of these observables below (above) neutron number 60, indicating an increase in deformation. The calculation reproduces well this trend and attributes it to a Type II QPT involving a jump between neutron number 58 and 60, from a weakly-deformed A configuration, to a strongly-deformed B configuration. This behavior is correlated with a similar jump seen for the $B(E2)$'s of $2^+ \rightarrow 0^+$ transitions in the even-even Zr cores, Fig. 3(c), and with the calculated order parameters, Fig. 3(b). The latter are the expectation value of \hat{n}_d in the 0^+_{1A} ground state wave function, $\langle \hat{n}_d \rangle_{0^+_{1A}}$, and in its Ψ_A and Ψ_B components, $\langle \hat{n}_d \rangle_A$, and $\langle \hat{n}_d \rangle_B$. Their evolution along the Zr chain reveals that configuration A remains spherical, while configuration B undergoes a Type I QPT involving a gradual spherical-to-deformed [U(5)-SU(3)-SO(6)] shape-phase transition.

Additional evidence for a Type I QPT, involving shape changes within the intruder B configuration, is obtained by examining the individual structure of Nb isotopes at the end-points of the region considered. Fig. 4 displays the experimental and calculated levels in ^{93}Nb along with $E2$ and $M1$ transitions among them. The corresponding spectra of ^{92}Zr , the even-even core, are also shown with an assignment of each level L to the normal A or intruder B configurations, based on the analysis in [7], which also showed that the two configurations in ^{92}Zr are spherical or weakly-deformed. It has long been known [29], that low-lying states of the A configuration in ^{93}Nb , can be interpreted in a weak coupling scheme, where the single-proton $\pi(1g_{9/2})$ state is coupled to spherical-vibrator states of the core. Specifically, for the 0^+_{1A} ground state of ^{92}Zr , this coupling yields the ground state $9/2^+$ of ^{93}Nb . For 2^+_{1A} , it yields a quintuplet of states, $5/2^+$, $7/2^+$, $9/2^+$, $11/2^+$, $13/2^+$, whose “center of gravity” (CoG) [30], is 0.976 MeV, in agreement with the observed

energy 0.935 MeV of 2^+_1 in ^{92}Zr . The $E2$ transitions from the quintuplet states to the ground state are comparable in magnitude to the $2^+_{1A} \rightarrow 0^+_{1A}$ transition in ^{92}Zr , except for $9/2^+$, whose decay is weaker. A nonet of states built on 4^+_{1A} can also be identified in the empirical spectrum of ^{93}Nb , with CoG of 1.591 MeV, close to 1.495 MeV of 4^+_{1A} .

Particularly relevant to the present discussion is the fact that the weak-coupling scenario is also valid for non-yrast states of the intruder B configuration in ^{93}Nb . As shown in Fig. 4, the coupling of $\pi(1g_{9/2})$ to the 0^+_{2B} state in ^{92}Zr , yields the excited $9/2^+$ state in ^{93}Nb . For 2^+_{2B} it yields

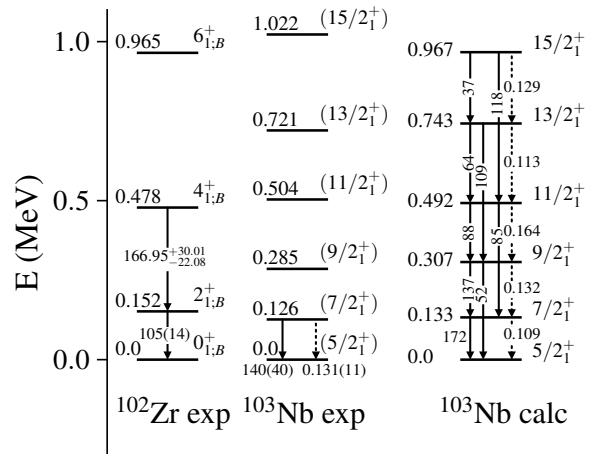


Figure 5. Experimental and calculated energy levels in MeV, and $E2$ (solid arrows) and $M1$ (dashed arrows) transition rates in W.u., for ^{103}Nb and ^{102}Zr . For the data, see Fig. 4 of [8].

the quintuplet, $5/2_3^+$, $7/2_3^+$, $9/2_4^+$, $11/2_3^+$, $13/2_2^+$, whose CoG is 1.705 MeV, a bit lower than 1.847 MeV of $2_{2,B}^+$. The observed $E2$ rates 1.03(9) W.u for $9/2_2^+ \rightarrow 9/2_1^+$, is close to the calculated value 0.85 W.u., but is smaller than the observed value 1.52(10) W.u for $9/2_3^+ \rightarrow 9/2_1^+$, suggesting that $9/2_2^+$ is associated with the B configuration.

For ^{103}Nb , the yrast states shown in Fig. 5 are arranged in a $K = 5/2^+$ rotational band, with an established [31] Nilsson model assignment $5/2^+$ [422]. The band members can be interpreted in the strong coupling scheme, where a particle is coupled to an axially-deformed core. The indicated states are obtained by coupling the $\pi(1g_{9/2})$ state to the ground band ($L = 0_{1,B}^+, 2_{1,B}^+, 4_{1,B}^+, 6_{1,B}^+, \dots$) of ^{102}Zr , also shown in Fig. 5, which is associated with the intruder B configuration. The calculations reproduce well the observed particle-rotor $J(J+1)$ splitting, as well as, the $E2$ and $M1$ transitions within the band. Altogether, we see an evolution of structure from weak-coupling of a spherical shape in ^{93}Nb , to strong-coupling of a deformed shape in ^{103}Nb . Such shape-changes within the B configuration (Type I QPT), superimposed on abrupt configuration crossing (Type-II QPT), are the key defining feature of intertwined QPTs. Interestingly, this intricate scenario, originally observed in the even-even Zr isotopes [5–7], persists in the adjacent odd-even Nb isotopes.

4 Conclusions

An application of the recently introduced IBFM-CM framework [8, 9] to Nb isotopes, disclosed a Type-II QPT (abrupt crossing of normal and intruder configurations) accompanied by a Type I QPT (gradual shape-evolution and transition from weak to strong coupling within the intruder configuration), thus demonstrating, for the first time, intertwined QPTs in odd-mass nuclei. The observed concurrent types of QPTs in odd-even Nb isotopes echo the intertwined QPTs previously found in the adjacent even-even Zr isotopes [5–7]. The results obtained motivate further experiments of non-yrast spectroscopy in such nuclei and their quantitative, yet physically transparent, description in the IBFM-CM framework.

This research was supported by the US-Israel Binational Science Foundation Grant No. 2016032.

References

- [1] A.E.L. Dieperink, O. Scholten and F. Iachello, Phys. Rev. Lett **44**, 1747 (1980).
- [2] P. Cejnar, J. Jolie and R. F. Casten, Rev. Mod. Phys. **82**, 2155 (2010).
- [3] A. Frank, P. Van Isacker and F. Iachello, Phys. Rev. C **73**, 061302(R) (2006).
- [4] K. Heyde and J. L. Wood, Rev. Mod. Phys. **83**, 1467 (2011).
- [5] N. Gavrielov, A. Leviatan and F. Iachello, Phys. Rev. C **99**, 064324 (2019).
- [6] N. Gavrielov, A. Leviatan and F. Iachello, Phys. Scr. **95**, 024001 (2020).
- [7] N. Gavrielov, A. Leviatan and F. Iachello, Phys. Rev. C **105**, 014305 (2022).
- [8] N. Gavrielov, A. Leviatan and F. Iachello, Phys. Rev. C **106**, L051304 (2022).
- [9] N. Gavrielov, Phys. Rev. C **108**, 014320 (2023).
- [10] F. Iachello and P. Van Isacker, *The Interacting Boson-Fermion Model*, (Cambridge Univ. Press, 1991).
- [11] F. Iachello and A. Arima, *The Interacting Boson Model* (Cambridge Univ. Press, 1987).
- [12] R.F. Casten, Prog. Part. Nucl. Phys. **62**, 183 (2009).
- [13] F. Iachello, Riv. Nuovo Cim. **34**, 617 (2011).
- [14] L. Fortunato, Prog. Part. Nucl. Phys. **121**, 103891 (2021).
- [15] O. Scholten and N. Blasi, Nucl. Phys. A **380**, 509 (1982).
- [16] D. Petrellis, A. Leviatan and F. Iachello, Ann. Phys. **326**, 926 (2011).
- [17] F. Iachello, A. Leviatan and D. Petrellis, Phys. Lett. B **705**, 379 (2011).
- [18] K. Nomura, T. Nikšić and D. Vretenar, Phys. Rev C **93**, 054305 (2016).
- [19] K. Nomura, T. Nikšić and D. Vretenar, Phys. Rev C **102**, 034315 (2020).
- [20] M. B  y  kata, C.E. Alonso, J.M. Arias, L. Fortunato and A. Vitturi, Symmetry **13**, 215 (2021) and references therein.
- [21] P. D. Duval and B. R. Barrett, Phys. Lett. B **100**, 223 (1981).
- [22] P. D. Duval and B. R. Barrett, Nucl. Phys. A **376**, 213 (1982).
- [23] M. Sambataro and G. Moln  r, Nucl. Phys. A **376**, 201 (1982).
- [24] J. E. Garc  a-Ramos and K. Heyde, Phys. Rev. C **89**, 014306 (2014).
- [25] K. Nomura, R. Rodr  guez-Guzm  n and L. M. Robledo, Phys. Rev. C **94**, 044314 (2016).
- [26] A. Leviatan, N. Gavrielov, J. E. Garc  a-Ramos and P. Van Isacker, Phys. Rev. C **98**, 031302(R) (2018).
- [27] J. E. Garc  a-Ramos and K. Heyde, Phys. Rev. C **100**, 044315 (2019).
- [28] R. Rodr  guez-Guzm  n, P. Sarriguren and L. M. Robledo, Phys. Rev. C **83**, 044307 (2011).
- [29] I.J. Van Heerden, W.R. McMurray and R. Saayman, Z. Physik **260**, 9 (1973).
- [30] R.D. Lawson and J.L. Uretsky, Phys. Rev. **108**, 1300 (1957).
- [31] M. A. C. Hotchkis *et. al.*, Nucl. Phys. A **530**, 111 (1991).